

Surface Excitations in Surface Electron Spectroscopies Studied by Reflection Electron Energy-Loss Spectroscopy and Elastic Peak Electron Spectroscopy

Takaharu NAGATOMI*† and Shigeo TANUMA**

*Department of Material and Life Science, Graduate School of Engineering, Osaka University, Suita, Osaka 565-0871, Japan

**Materials Analysis Station, National Institute for Materials Science, 1-2-1 Sengen, Tsukuba, Ibaraki 305-0047, Japan

Surface excitations, in addition to bulk excitation, undergone by signal electrons in surface electron spectroscopies, such as Auger electron spectroscopy, and X-ray photoelectron spectroscopy, play an important role in the formation of electron spectra. Those inelastic scattering processes not only induce decay in the peak intensity, but also form background appearing in the lower kinetic energy side of relevant peaks. Information on surface excitation is essential in addition to bulk excitations for the quantification of material surfaces by surface electron spectroscopies, and extensive studies have been devoted to it. In this report, we introduce the basics of the study of surface excitations by reflection electron energy loss spectroscopy (REELS) and elastic peak electron spectroscopy (EPES). The application of several approaches within the schemes of EPES analysis and REELS analysis to the experimental determination of inelastic scattering parameters, such as the surface excitation parameter (SEP), differential SEP (DSEP), inelastic mean free path (IMFP), and dielectric function, are also introduced. Information useful to calculate the values of the IMFP and SEP using predictive equations is provided in Supporting Information as well.

(Received October 2, 2009; Accepted December 26, 2009; Published February 10, 2010)

1 Introduction	165	4 REELS Analysis	170
2 Surface Excitation	166	4-1 Tougaard method	
2-1 Basics of EPES analysis		4-2 Partial intensity approach	
2-2 Absolute EPES analysis		4-3 Absolute REELS analysis	
2-3 SEP and DSEP		5 Summary	175
3 EPES Analysis	169	6 Acknowledgements	175
3-1 Determination of IMFP		7 Supporting Information	175
3-2 Determination of SEP		8 References	175

1 Introduction

Surface electron spectroscopies, such as Auger electron spectroscopy (AES) and X-ray photoelectron spectroscopy (XPS), have been widely used for characterization of material surfaces. In such electron spectroscopies, signal electrons, the typical kinetic energy of which is 50 to 3000 eV, strongly interact with solids, and interactions cause scattering of signal electrons. There are two types of scattering, *i.e.*, elastic and inelastic scatterings. Elastic scattering causes an angular deflection of the moving direction of signal electrons, and inelastic scattering induces an energy loss of signal electrons through various kinds of inelastic scattering channels. Because

of strong interactions between the solid and electrons, most signal electrons undergo multiple scattering events, and only a few generated near the surface region are detected as Auger or photoelectron peaks without losing their kinetic energy during transport in a solid. The signal electrons detected after losing their kinetic energy are observed as a background in the spectra. Therefore, a comprehensive understanding of the interaction of signal electrons with solids is essential for the quantitative characterization of material surfaces using surface electron spectroscopies.

Interactions of electrons with a solid surface are described by relevant scattering parameters. Elastic scattering can be described by the differential elastic scattering cross-section (DECS) and the elastic mean free path (EMFP). Inelastic scattering phenomena can be divided into two kinds of scattering. One is bulk excitation and the other is surface excitation. Bulk excitation is defined as the excitation of modes

† To whom correspondence should be addressed.
E-mail: nagatomi@mls.eng.osaka-u.ac.jp

in the bulk, *e.g.*, bulk plasmon excitation, interband transition, and ionization. Surface excitation is the excitation of modes localized near the solid surface, such as surface plasmon excitation. Bulk excitation is described using well-known parameters of the inelastic mean free path (IMFP) and differential inverse mean free path (DIMFP). Similar to bulk excitation, surface excitation is characterized by the surface excitation parameter (SEP) and the differential SEP (DSEP). Since these scattering parameters are required for a quantitative surface chemical analysis using AES and XPS, the analysis of the spectrum intensity and shape has been extensively performed in order to experimentally determine those parameters, and databases of those parameters have been intensively constructed.

In the present report, we reviewed the experimental determination of parameters describing inelastic scattering, particularly surface excitations, using the background shape analysis of reflection electron energy loss spectroscopy (REELS) and elastic peak electron spectroscopy (EPES). First, we introduce a physical description of these scattering parameters (several parts of them are described in Supporting Information) and the basics of analytical approaches. We then describe several approaches to experimentally determine the scattering parameters, such as SEP, DSEP, and IMFP and introduce their results.

2 Surface Excitation

2.1 Basics of EPES analysis

In the EPES analysis, the intensity of electrons elastically backscattered from the sample surface is measured as a function of, *e.g.*, the primary energy of electrons. As easily found from Fig. S4 (Supporting Information), showing schematic of the Landau theory, the intensity of the elastic peak, *i.e.*, the no-loss peak at $\Delta\varepsilon = 0$, where $\Delta\varepsilon$ is the energy loss, exponentially decreases according to the IMFP with increasing its path length. Therefore, EPES analysis is one of the recommended methods for measuring IMFPs, and details of this technique are reviewed.¹⁻³ Here, the basic concepts of EPES are briefly described.

The moving directions of primary electrons are changed by elastic scattering. The *i*th segment of the path length between the (*i* - 1)th and *i*th successive elastic scattering events of *j*th primary electron is defined as $s_{j,i}$. If the *j*th electron undergoes i_j' times elastic scattering before being emitted from the surface into the vacuum, the total path length, s_j , of the *j*th electron is given by $s_j = \sum_{i=0}^{i_j'} s_{j,i}$. Then, according to the definition of the IMFP, λ_{in} , the ratio of the measured intensity of the elastic peak, I_{el} , to the intensity of primary electrons after the irradiation of N_0 electrons is expressed as

$$I_{el} = \frac{T}{N_0} \sum_{j=1}^{N_0} \exp\left(-\frac{s_j}{\lambda_{in}}\right) = \frac{T}{N_0} \sum_{j=1}^{N_0} \exp\left(-\frac{\sum_{i=0}^{i_j'} s_{j,i}}{\lambda_{in}}\right), \quad (1)$$

where T is the transmission function of the analyzer and Σ' means that summation over *j* is made only for electrons detected by the analyzer. In a practical application of the EPES analysis to the determination of the IMFP using Eq. (1), the path length distribution could be calculated by a Monte Carlo (MC) simulation.

When the path length distribution of detected electrons, $d\eta/ds$, per electron is calculated by the MC simulation, in which

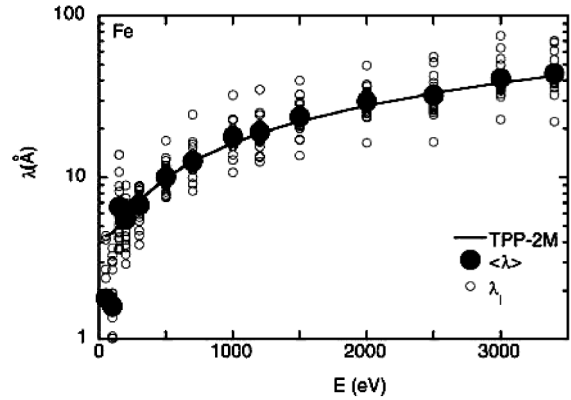


Fig. 1 IMFP, λ_{in} , for Fe determined by the EPES analysis using 23 reference samples.⁴ (Reprinted from Ref. 4, Copyright (2000), with permission from Elsevier.)

electron trajectories are traced by taking into account only elastic scattering, the ratio of the elastic peak intensity to the intensity of primary electrons, I_{el} , is given by

$$I_{el} = \frac{T}{N_0} \int_0^{\infty} \frac{d\eta}{dx} \exp\left(-\frac{x}{\lambda_{in}}\right) dx. \quad (2)$$

By fitting the calculated I_{el} , in which the IMFP, λ_{in} , is a fitting parameter, with the experimental I_{el} , the IMFP can be determined. However, because of difficulty in the accurate measurement of T in Eq. (2), the determination of the IMFP by a direct comparison of the calculated and experimental I_{el} is difficult. Therefore, the determination of the IMFP by EPES analysis is usually performed using reference samples. When I_{el} for the sample is normalized by that for the reference sample, *i.e.*,

$$\frac{(I_{el})_{\text{sample}}}{(I_{el})_{\text{reference}}} = \frac{\int_0^{\infty} \left(\frac{d\eta}{dx}\right)_{\text{sample}} \exp\left(-\frac{x}{\lambda_{in}^{\text{sample}}}\right) dx}{\int_0^{\infty} \left(\frac{d\eta}{dx}\right)_{\text{reference}} \exp\left(-\frac{x}{\lambda_{in}^{\text{reference}}}\right) dx}, \quad (3)$$

the effects of T can be canceled out. It should be noted that the EPES analysis using Eq. (3) requires the value of the IMFP of the reference sample, $\lambda_{in}^{\text{reference}}$, to be known. This means that the value of the IMFP of the sample, $\lambda_{in}^{\text{sample}}$, determined by the EPES analysis using the reference sample depends on the selection of the reference sample and the value of $\lambda_{in}^{\text{reference}}$.

Figure 1 shows the IMFP of Fe determined by EPES analysis, where 23 elemental solids were used as reference samples.⁴ Solid circles show the values of the IMFP averaged over the entire data set at one energy. A relatively good agreement of IMFPs between those obtained by averaging data of the EPES analysis and those calculated using the TPP-2M predictive equation is observed. This result indicates that averaging the values of the IMFP obtained using different reference samples is effective to measure IMFP using EPES analysis. Note that a large scatter of the data is confirmed. This might be attributed to the values of the IMFPs used for the references. A part of the reason for the large scatter of data might be due to the dependence of surface excitations on elements, where effects of surface excitations are neglected in Eq. (3). Note that the use of a subset of reference materials recommended for the EPES

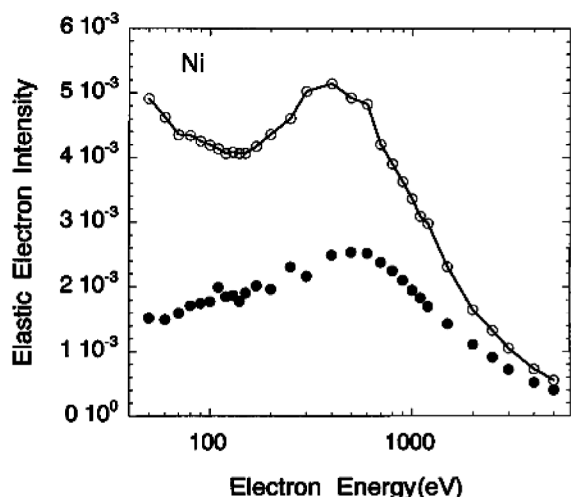


Fig. 2 Absolute elastic peak intensities reflected from the Ni surface.⁶ Solid circles show the experimental elastic peak intensities. Open circles represent the elastic peak intensities calculated by the MC simulation without taken into account effects of surface excitations, *i.e.*, $f_s = 1$ in Eq. (14) (see text in Sec. 2-3). (Reprinted from Ref. 6, Copyright (2000), with permission from John Wiley & Sons Limited.)

analysis (Au, Ag, Cu, and Ni)¹ results in a smaller scatter among the IMFP values for unknown samples, which are determined by the EPES analysis.⁵

2-2 Absolute EPES analysis

In EPES analysis for determining the IMFP values, a reference sample is required to cancel out the effect of the transmission function, T , as mentioned in the Sec. 2-1. In contrast, when the elastic peak intensity is measured with absolute units, the EPES analysis can be performed using Eq. (2) without reference samples. One of the authors (S. T.)⁶ performed the EPES analysis of elastic peak intensities absolutely measured using a noble cylindrical mirror analyzer (CMA), the detector of which was a Faraday cup, enabling direct measurement of the electron current due to the signal electrons.^{7,8}

Figure 2 shows the elastic peak intensity reflected from the Ni surface as a function of the primary energy of the electrons.⁶ It is clearly found that the experimentally obtained absolute elastic peak intensities are significantly lower than those obtained by the MC simulation, in which the values of the IMFP calculated using the TPP-2M predictive equation were employed. An overestimation of the elastic peak intensity by the MC simulation is more significant for a lower electron energy. The overestimation of the elastic peak intensity by the MC simulation can be attributed to neglecting effects of surface excitations in Eq. (2), where surface excitations cause a decrease in the elastic peak intensity in the experiment. The results shown in Fig. 2, obtained by the absolute EPES analysis, revealed that the decay of the peak intensity by surface excitations reaches to 80% at maximum and that care for surface excitations is required for quantification by surface electron spectroscopies.

2-3 SEP and DSEP

The effects of surface excitations on the decay of the elastic peak intensity are significant as confirmed in Fig. 2, and the decay of the peak intensity by surface excitations is described by the SEP. The energy-loss distribution by surface excitations is given by the DSEP. Here, we briefly explain the SEP and

DSEP.

By assuming that the DIMFP can be divided into components due to bulk and surface excitations, $K_b(E, \Delta E)$ and $K_s(E, \Delta E, \alpha, z)$,⁹⁻¹¹ the DIMFP, in which the contribution of surface excitations to energy loss processes is taken into account, may be given as

$$K(E, \Delta E, \alpha, z) = K_b(E, \Delta E) + K_s(E, \Delta E, \alpha, z). \quad (4)$$

Here, the DIMFP, $K(E, \Delta E, \alpha, z)$, depends on the depth, z , and the angle of emission, α , when surface excitations are taken into account, since a probability of surface excitations depends on z and α . The surface exists at $z = 0$, and $z > 0$ and $z < 0$ correspond to the vacuum and inside solid, respectively. The z -dependent DIMFP for deep inside the solid is given by

$$K(E, \Delta E, \alpha, z = -\infty) = K_b(E, \Delta E), \quad (5)$$

since the DIMFP due to surface excitations, $K_s(E, \Delta E, \alpha, z)$, is zero deep inside the solid. When an electron exists outside the solid, only surface excitations contribute to the z -dependent DIMFP,

$$K(E, \Delta E, \alpha, z > 0) = K_s(E, \Delta E, \alpha, z > 0). \quad (6)$$

The surface excitations are significant only near the surface region. The surface zone, where energy-loss processes due to surface excitations play an important role, can be roughly estimated from $\sim \nu/\omega$, where ν is the speed of electrons and $\hbar\omega$ is the energy of the surface plasmon. When the typical energy of the surface plasmon of $\hbar\omega = 12$ eV and the electron energy of 1 keV are considered, the thickness of the surface zone is estimated to be ~ 10 Å. Since the IMFP of 1 keV electrons is approximately 20 Å, the contribution of surface excitations in the vicinity of the surface is considered to be significant.

Figures 3 and 4 show the z -dependent DIMFPs of 1 keV electrons for Cu at $\alpha = 0^\circ$, which are theoretically calculated, when an electron is inside and outside the solid, respectively.¹¹ For an electron inside the solid (Fig. 3), the shapes of the DIMFP are different between those for electrons near the surface and deep inside the solid. In addition, the intensity of the z -dependent DIMFP in the low-energy loss region is higher for electrons existing near the surface region. When an electron is in vacuum (Fig. 4), the DIMFP consists of the component due to only surface excitations. The shape of the DIMFP does not significantly depend on the distance from the surface, z , so much, and only the intensity strongly depends on z . The background of the electron spectrum is determined by the DIMFP as mentioned in Sec. S1-3 in Supporting Information and the shape of the z -dependent DIMFP is significantly different from the DIMFP for only bulk excitations, indicating that the energy loss structure observed in the background at the lower kinetic energy side of peaks is modified by surface excitations.

Although the z -dependent DIMFP is more accurate, its z -dependence significantly limits its application to a practical use. Therefore, the DSEP obtained by integrating the component of the z -dependent DIMFP due to surface excitations over the depth, z , is more convenient, *i.e.*,¹⁰

$$K_s(E, \Delta E, \alpha) = \int_{-\infty}^{\infty} K_s(E, \Delta E, \alpha, z) \frac{dz}{\cos \alpha}, \quad (7)$$

and, then, Eq. (4) is rewritten as

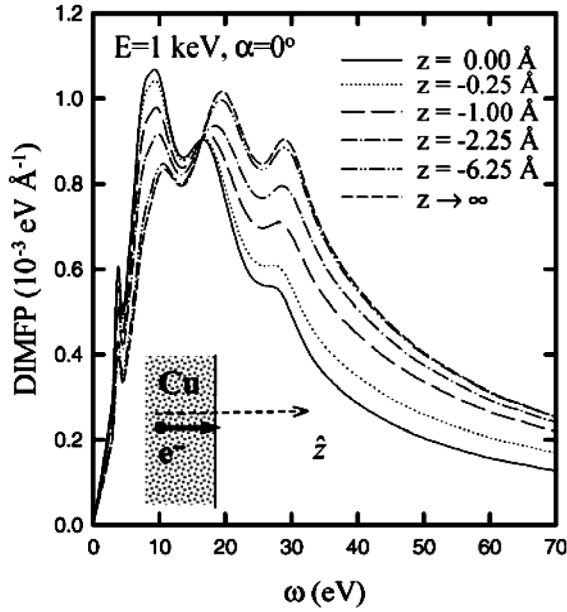


Fig. 3 Theoretically calculated z -dependent DIMFP, $K(E, \Delta E, \alpha, z)$, of 1 keV electrons inside Cu at $\alpha = 0^\circ$.¹¹ (Reprinted from Ref. 11, Copyright (2002), with permission from Elsevier.)

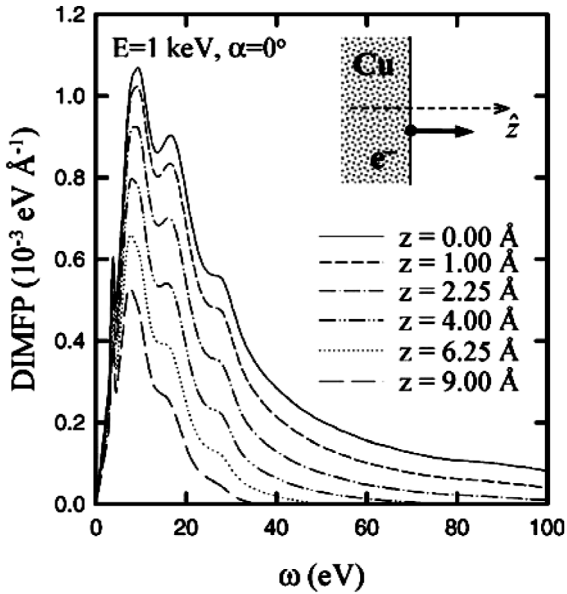


Fig. 4 Theoretically calculated z -dependent DIMFP, $K(E, \Delta E, \alpha, z)$, of 1 keV electrons outside Cu at $\alpha = 0^\circ$.¹¹ (Reprinted from Ref. 11, Copyright (2002), with permission from Elsevier.)

$$K(E, \Delta E, \alpha) = K_b(E, \Delta E) + K_s(E, \Delta E, \alpha). \quad (8)$$

Here, $K_s(E, \Delta E, \alpha)$ is the DSEP and describes the probability that an electron crossing the surface at an angle of α loses an energy of ΔE per unit energy loss by a single surface excitation event. Figure 5 shows the DSEP for Ni calculated using the Tung's model, in which the DSEP is given in atomic units as¹²

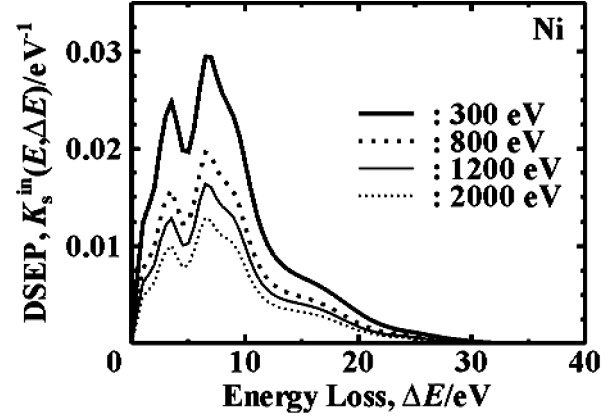


Fig. 5 DSEP for Ni theoretically calculated using Tung's model.¹²

$$K_s^{\text{Tung}}(\omega) = K_s^+(\omega) + K_s^-(\omega), \quad (9a)$$

$$K_s^\pm(\omega) = \frac{2}{\pi v^2 \cos \alpha} \int_{k^-}^{k^+} \frac{k_s'}{k^3} \text{Im} \left[\frac{(\epsilon - 1)^2}{\epsilon(\epsilon + 1)} \right] dk, \quad (9b)$$

$$k_s' = \left[k^2 - \left(\frac{\omega}{v} + \frac{k^2}{2v} \right)^2 \right]^{1/2} \cos \alpha \pm \left(\frac{\omega}{v} + \frac{k^2}{2v} \right) \sin \alpha, \quad (9c)$$

$$k_s^\pm = \sqrt{2E_0} \pm \sqrt{2(E_0 - \omega)}. \quad (9d)$$

For calculating the DSEP, the dielectric function, $\epsilon(k, \omega) = \epsilon_1(k, \omega) + i\epsilon_2(k, \omega)$, modeled by fitting a Drude-Lindhard type of expansion to optical data was used,¹²

$$\epsilon_1(k, \omega) = \epsilon_b - \sum_i \frac{A_i [\omega^2 - (\omega_i + k^2/2)^2]}{[\omega^2 - (\omega_i + k^2/2)^2]^2 + \omega^2 \gamma_i^2}, \quad (10a)$$

$$\epsilon_2(k, \omega) = \sum_i \frac{A_i \gamma_i \omega}{[\omega^2 - (\omega_i + k^2/2)^2]^2 + \omega^2 \gamma_i^2}, \quad (10b)$$

where the parameters in Eq. (10) for Ni are taken from the literature.¹³ It is clearly seen that the intensity of the DSEP is higher for a lower electron energy. In addition, a comparison of the DIMFP only for bulk excitation shown in Fig. S3 (Supporting Information) revealed that surface excitations tend to cause a lower energy loss than bulk excitations.

For practical applications, a further integration of the DSEP over the energy loss, ΔE , is useful,

$$P_s(E, \alpha) = \int_0^{E_0} K_s(E, \Delta E, \alpha) d(\Delta E), \quad (11)$$

where $P_s(E, \alpha)$ is the SEP describing the average number of surface excitation events undergone by an electron when the electron crosses the surface. Figure 6 shows the theoretically calculated SEP for Au.⁹ With an increase in α and a decrease in the electron energy, E , SEP increases.

With the assumption that the surface excitation obeys the Poisson stochastic process, the probability that an electron participates in the l -fold surface excitation events, P_l , is given by the SEP as

$$P_l = \frac{1}{l!} P_s(E, \alpha)^l \exp[-P_s(E, \alpha)]. \quad (12)$$

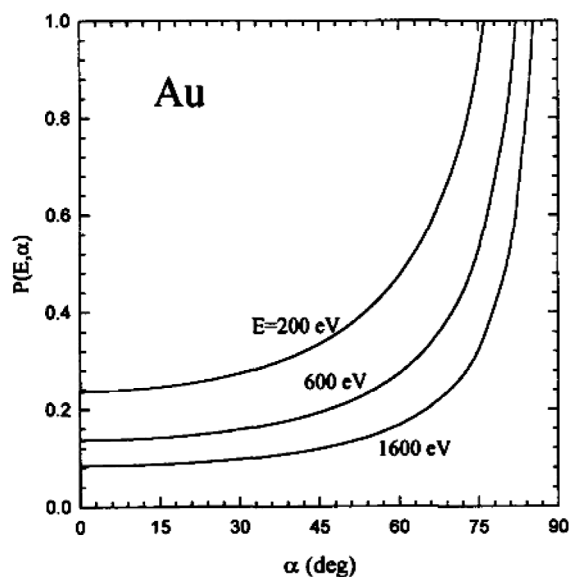


Fig. 6 Theoretically calculated values of the SEP for Au.⁹ (Reprinted from Ref. 9, Copyright (1996), with permission from Elsevier.)

Then, the probability that an EPES electron crosses the surface without undergoing surface excitations, f_s , is

$$f_s = \exp[-P_s(E, \alpha_{in})] \exp[-P_s(E, \alpha_{out})], \quad (13)$$

and the elastic peak intensity given by Eq. (2) is

$$I_{el}' = f_s T \int_0^\infty \frac{d\eta}{dx} \exp\left(-\frac{x}{\lambda_{in}}\right) dx. \quad (14)$$

Here, α_{in} and α_{out} are the surface crossing angles of an electron on its incoming and outgoing ways in the EPES measurement. Then, Eq. (3) for the EPES analysis using the reference sample is also modified as

$$\frac{(I_{el}')_{sample}}{(I_{el}')_{reference}} = \frac{f_s^{sample} \int_0^\infty \left(\frac{d\eta}{dx}\right)_{sample} \exp\left(-\frac{x}{\lambda_{in}^{sample}}\right) dx}{f_s^{reference} \int_0^\infty \left(\frac{d\eta}{dx}\right)_{reference} \exp\left(-\frac{x}{\lambda_{in}^{reference}}\right) dx}. \quad (15)$$

Equations (14) and (15) are the basic equations for EPES analysis when the contribution of surface excitations to the decrease of the elastic peak intensity is taken into account.

3 EPES Analysis

As mentioned above, EPES analysis is one of the methods recommended for experimentally determining the IMFP values.¹⁻³ In addition, this technique can be applied to determining the SEP values. In this section, several attempts to determine the IMFP and SEP by the EPES analysis are briefly introduced.

3-1 Determination of IMFP

As an example of the application of EPES analysis to the determination of IMFP, the experimental determination of IMFP using a reference sample is briefly described. Figure 7 shows

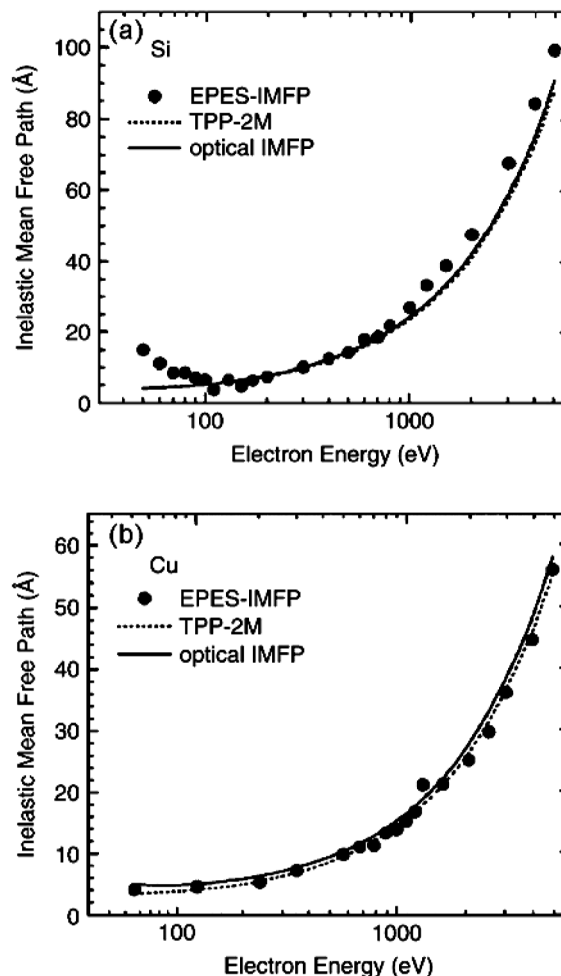


Fig. 7 IMFP values for (a) Si and (b) Cu determined by the EPES analysis using Ni as a reference.¹⁴ (Reprinted from Ref. 14, Copyright (2005), with permission from John Wiley & Sons Limited.)

IMFP values for Si and Cu determined by the EPES analysis using Eq. (3).¹⁴ The experimental elastic peak intensities used for the analysis were those measured absolutely.^{7,8} An elemental solid used for a reference was Ni, which is one of the recommended elements as a reference sample of EPES analysis.¹ The experimentally determined values of IMFP were compared with those calculated using the TPP-2M predictive equation and those theoretically calculated from optical data within a scheme of the dielectric response theory (optical IMFP). It is clearly found that the EPES IMFP values for Si and Cu using Ni as a reference show reasonable agreements with those of the TPP-2M equation and the optical IMFP. It should be noted that the discrepancy between the experimentally determined IMFP values and the TPP-2M equation is slightly larger for Si than that for Cu. This could be attributed to the fact that effects of surface excitations are neglected in this EPES analysis.¹⁴

As mentioned in Sec. 2-2, the effects of surface excitations on the elastic peak intensity in the EPES measurement is significant, and the correction for surface excitations is required for accurate EPES analysis. Several authors have determined IMFP values using Eq. (15) with a correction for surface excitations.^{15,16} Figure 8 shows an example of the determination of IMFP values for Si by the EPES analysis with and without any correction for surface excitations.¹⁵ The SEP values used for the correction were taken from the literature.¹⁷ It is clear that the IMFP values

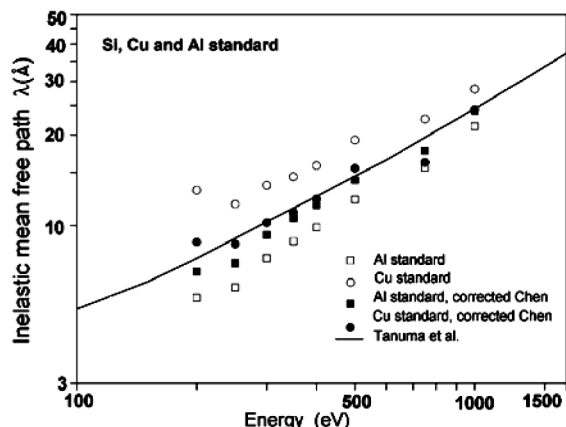


Fig. 8 IMFP values for Si determined by the EPES analysis.¹⁵ Solid and open symbols represent the IMFP values obtained with and without a surface excitation correction. Squares and circles are the IMFP values determined using Al and Cu as references. The solid line shows the IMFP calculated from optical data.¹⁸ (Reprinted from Ref. 15, Copyright (2003), with permission from Elsevier.)

for Si determined without any correction for surface excitations show a large deviation from those calculated using optical data.¹⁸ The IMFP values determined with the surface excitation correction agree well with the optical one for both references of Al and Cu. These results strongly suggest that the EPES analysis for the determination of the IMFP should be performed with taking into account a correction for surface excitations. The obtained IMFP values depend on the reference sample and their IMFP and SEP used for EPES analysis. When the IMFP values are determined for a sample, the use of a reference material, for instance, the SEP of which is expected to be similar to the sample, is recommended in order to reduce the error introduced by the dependence of the SEP on the reference sample.

3-2 Determination of SEP

Since the elastic peak intensity in the EPES measurement is strongly affected by surface excitations, the determination of SEP by EPES analysis using Eqs. (14) or (15) is possible. Figure 9 shows the total of the SEP values, which is given as a sum of the SEP for incoming and outgoing electrons in the EPES experiment, determined by the absolute EPES analysis using Eq. (14).⁶ The values of the IMFP required for the EPES analysis were taken from literature.¹⁸ The obtained SEP values are found to be larger than those calculated by Chen's¹⁹ and Oswald's²⁰ equations originally reported for a free-electron metal. The total SEP values for electrons below 1 keV is found to be 0.5 to 1. This indicates that the average number of surface excitation events, in which most of signal electrons emitted from the Ni surface in AES and XPS measurements participate, is 0.25 to 0.5, revealing that the contribution of surface excitations in surface electron spectroscopies is significant. It should be noted that this approach is a unique EPES technique that does not require any reference materials, though the IMFP value of the sample should be known.

Several attempts have been made to determine SEP by EPES analysis using the reference materials and Eq. (15).^{16,21} These results revealed that the SEP values can be reasonably obtained by EPES analysis. Note that the obtained SEP values strongly depend on the reference materials, *i.e.*, the values of IMFP and SEP used in the analysis.

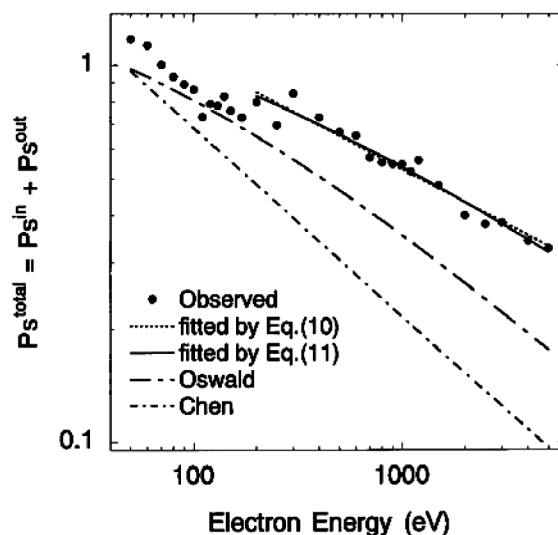


Fig. 9 Total SEPs for Ni, which is given as a sum of the SEP values for incoming and outgoing electrons, determined by absolute EPES analysis.⁶ Curves labeled by Chen and Oswald represent the values of the SEP calculated by Chen's¹⁹ and Oswald's²⁰ equations, both of which were proposed for a free-electron metal. For curves fitted by Eqs. (10) and (11) in this figure, see Fig. 6 of Ref. 6. (Reprinted from Ref. 6, Copyright (2000), with permission from John Wiley & Sons Limited.)

4 REELS Analysis

The analysis of REELS spectra also provides powerful approaches to investigate the inelastic interaction of signal electrons with a solid surface in surface electron spectroscopies. In REELS analysis, inelastic scattering parameters, such as SEP, and DSEP, can be determined from the elastic peak intensity and the energy-loss spectrum. Analytical approaches to deduce such parameters from REELS spectra are based on the Landau theory described in Sec. S1-3 in Supporting Information. In this section, we briefly describe several analytical approaches to deduce inelastic scattering parameters from REELS spectra.

4-1 Tougaard method

The Tougaard method has been used for background subtraction and surface compositional analysis in surface electron spectroscopies. In this article, we mainly focus on the application of the Tougaard method to the determination of scattering parameters related to surface excitations. The most simplified issue in this approach is that a REELS electron has a V-shape trajectory, so that all of the signal electrons undergo only single large-angle elastic scattering event in the sample.

The REELS analysis by the Tougaard method is based on an analytical equation,^{22,23}

$$\lambda^* K_{\text{exp}}(E_0, E_0 - E) = \frac{j_1(E) - \int_E^{E_0} \lambda^* K_{\text{exp}}(E_0, E' - E) j_1(E') dE'}{A_0}, \quad (16)$$

where $\lambda^* = \lambda_{\text{in}} L / (\lambda_{\text{in}} + L)$ and L is the parameter to take into account the effects of elastic scattering, and is typically given as $2\lambda_{\text{tr}}$. $E_0 - E$ is the energy loss, ΔE . $j_1(E)$ is the REELS spectrum. A_0 is the elastic peak area. $K_{\text{exp}}(E_0, E_0 - E)$ is the experimentally determined DIMFP, which effectively takes into account both surface and bulk excitations. In this approach, localization of

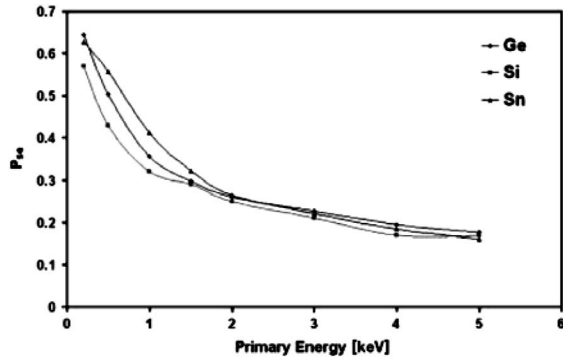


Fig. 10 SEP values for Ge, Si, and Sn, determined by deconvolution of the experimentally determined DIMFP, $K_{\text{exp}}(E_0, E_0 - E)$, by the Tougaard method.²⁶ (Reprinted from Ref. 26, Copyright (2002), with permission from John Wiley & Sons Limited.)

the surface excitation in the near-surface region is not considered, and all of the energy loss processes are assumed to occur in the same manner without distinguishing bulk and surface excitation processes.

Since $K_{\text{exp}}(E_0, E_0 - E)$ effectively includes contributions of both surface and bulk excitations, the determination of SEP values by deconvoluting $K_{\text{exp}}(E_0, E_0 - E)$ into components due to bulk and surface excitations has been performed.²⁴⁻²⁶ Figure 10 shows SEP values for Ge, Si, and Sn, determined by deconvolution of the experimentally determined DIMFP, $K_{\text{exp}}(E_0, E_0 - E)$, by the Tougaard method.²⁶ In this approach, the DIMFP, $K_{\text{exp}}(E_0, E_0 - E)$, was first determined from the REELS spectra by the Tougaard method. Then, by assuming that the bulk component of the DIMFP is described by the Tougaard's universal curve,²⁷ $K_{\text{exp}}(E_0, E_0 - E)$ was deconvoluted into the components due to surface and bulk excitations according to Eq. (8). Finally, integration of the component due to surface excitations over the energy loss is performed, and the ratio of the integrated component of surface excitations to that of the bulk component provides the SEP²⁶ which is shown in Fig. 10. It is found that the SEP increases with a decrease in the electron energy for all elements. Note that this approach is applicable only for the system, where the profile of the bulk plasmon loss peak in the REELS spectra from samples is relatively sharp.

As a similar approach, the application of factor analysis to the deconvolution of $K_{\text{exp}}(E_0, E_0 - E)$ into the components due to bulk and surface excitations has recently been investigated.²⁸⁻³⁰ Factor analysis of a series of REELS spectra measured for Si at different primary energies and detection angles successfully results in the deconvolution of $K_{\text{exp}}(E_0, E_0 - E)$ into components due to surface and bulk excitations. An evaluation of the SEP values for Si has been reported.³⁰ A determination of the dielectric function from the component of the DIMFP for bulk excitations has also been reported.³⁰

Another approach to study surface excitations based on the Tougaard method is a theoretical calculation of the effective DIMFP, in which both the surface and bulk excitations are taken into account, using the specular reflection model under the assumption that a REELS electron has a V-shape trajectory (Yubero-Tougaard theory).³¹ The theoretically calculated effective DIMFPs have been confirmed to show a reasonable agreement with the experimentally determined DIMFP, $K_{\text{exp}}(E_0, E_0 - E)$, using the Tougaard method.³² Recently, these techniques have been applied to the determination of the energy-loss function, *i.e.*, the imaginary part of the inverse of

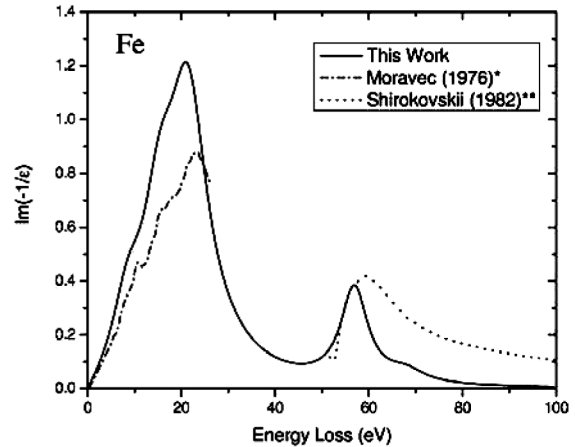


Fig. 11 Energy-loss function for Fe determined by the Yubero-Tougaard theory.³³ Reference data of Moravec (1976)³⁵ and Shirokovskii (1982)³⁶ are taken from Palik optical data.³⁷ (Reprinted from Ref. 33, Copyright (2008), with permission from the American Physical Society.)

the dielectric function, $\text{Im}(-1/\epsilon)$, by an iteration procedure, in which the calculation of the theoretical DIMFP is repeated by changing the dielectric function as fitting parameters until the calculated one is in a good agreement with the experimental one, $K_{\text{exp}}(E_0, E_0 - E)$.^{33,34}

Results on the determination of the energy loss function and the DIMFP for Fe^{33,34} are shown in Figs. 11 and 12 as examples. It is clear for the energy-loss function shown in Fig. 11 that the agreement with Palik optical data is reasonable for $\Delta E < 30$ eV, while the agreement is not good for $\Delta E > 30$ eV. This must be attributed to the fact that Palik optical data for Fe in the $\Delta E > 30$ eV and $\Delta E > 30$ eV energy regions were taken from different literatures, and that those data are 25 - 40 years old, which may have experimental uncertainties caused by, *e.g.*, surface contamination. The DIMFP shown in Fig. 12 revealed that the agreement between theory and experiment is quite good for all angles and energies for each material, and the experimentally observed variation with the angle and the energy is well described by theory, in which newly determined optical data shown in Fig. 11 was used for the calculation. This method is believed to be one of the effective approaches to measure the dielectric function experimentally for the energy-loss region of 0 to 100 eV using the REELS measurement.

4.2 Partial intensity approach

In the partial intensity approach, the background of a REELS spectra are deconvoluted into components due to electrons that undergo n -fold inelastic scattering events using the partial intensity, C_n .^{17,38-42} Let the number of surface and bulk excitation events, n_B and n_S , respectively, a REELS spectrum, $J(E)$, is given by

$$J(E) = \sum_{n_B=0}^{\infty} \sum_{n_S=0}^{\infty} C_{n_B} C_{n_S} L_{n_B, n_S}(\Delta E) \otimes F(E + \Delta E). \quad (17)$$

Here, \otimes represents the convolution, and $F(E + \Delta E)$ is the energy distribution of primary electrons in the REELS measurement. $L_{n_B, n_S}(\Delta E)$ is the energy-loss distribution of an electron after undergoing n_B -fold bulk and n_S -fold surface excitation events, and is given by

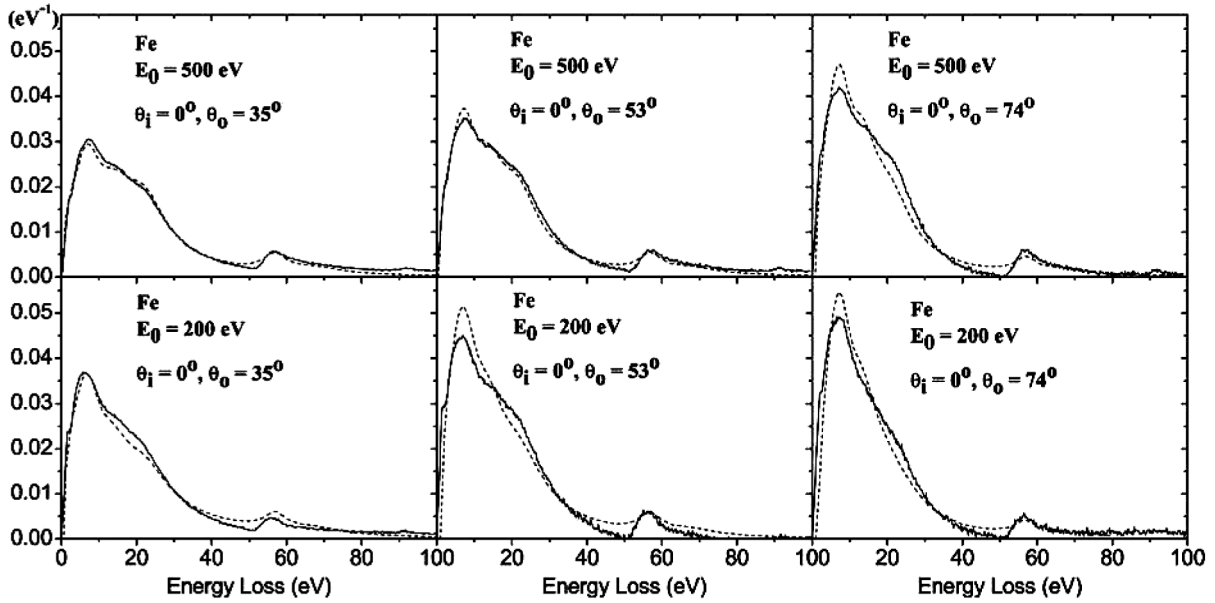


Fig. 12 Experimentally determined DIMFP, $\lambda^*K_{\text{exp}}(E_0, E_0 - E)$, in which the contributions of both surface and bulk excitations are taken into account, by the Yubero-Tougaard theory (solid line) and the DIMFP theoretically calculated by the Yubero-Tougaard theory using the energy loss function shown in Fig. 11 (dashed line), which is determined by fitting the theoretical DIMFP with the experimental one.^{33,34} (Reprinted from Ref. 34, Copyright (2008), with permission from the American Physical Society.)

$$L_{n_b, n_s}(\Delta E) = \int L_{n_b}(\Delta E - \Delta E') L_{n_s}(\Delta E') d(\Delta E'), \quad (18a)$$

where $L_{n_b}(\Delta E) = L_{n_b,0}(\Delta E)$, $L_{n_s}(\Delta E) = L_{0, n_s}(\Delta E)$, and $L_{0,0}(\Delta E) = \delta(\Delta E)$. $L_{n_b}(\Delta E)$ and $L_{n_s}(\Delta E)$ are the n_b -fold convolution of the normalized DIMFP (normalized to unit area) for bulk excitations and the n_s -fold convolution of the normalized DSEP (normalized to unit area), respectively, *i.e.*,

$$L_{n_b}(\Delta E) = [\lambda_{\text{in}} K_b(E, \Delta E)]^{\otimes n_b} [\lambda_{\text{in}} K_b(E, \Delta E)], \quad (18b)$$

$$L_{n_s}(\Delta E) = [P_s(E, \alpha)^{-1} K_s(E, \Delta E, \alpha)]^{\otimes n_s} [P_s(E, \alpha)^{-1} K_s(E, \Delta E, \alpha)], \quad (18c)$$

where \otimes^n represents the n -fold convolution. By deconvoluting the REELS spectrum according to Eqs. (17) and (18), the SEP and DSEP can be determined by providing the IMFP value as input data. Within the scheme of the partial intensity approach, SEP is given by

$$P_s(E, \alpha) = \frac{C_{n_b=0} C_{n_s=1}}{C_{n_b=0} C_{n_s=0}}. \quad (19)$$

Note that the multiple scattering events are taken into account in the partial intensity analysis. For this, the analysis was performed with the help of an MC simulation. The MC simulation was used to calculate the partial intensity for the bulk excitation, C_{n_b} .

Figure 13 shows the results of the analysis of the REELS spectra for (a) Si and (b) Ni by the partial-intensity approach.⁴⁰ The components due to electrons participating in the single surface excitation event is plotted by the dotted line. The decrease in the intensity of energy losses due to surface excitations is confirmed with the increase of the electron energy. For Si, the shape of the component of single-surface excitation

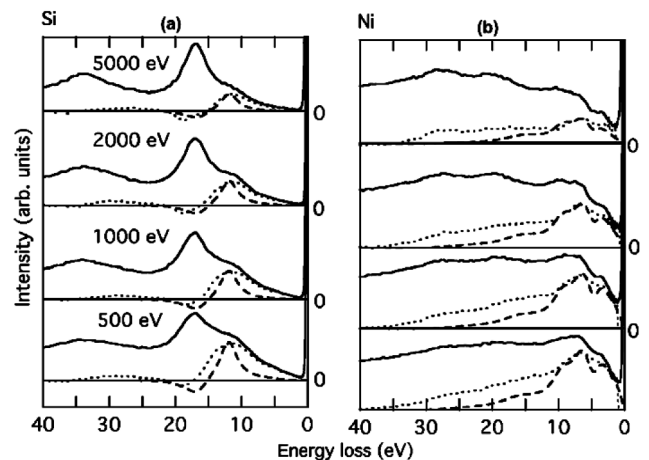


Fig. 13 REELS spectra at the primary energies of 500, 1000, 2000, and 5000 eV, and its analysis by the partial-intensity approach for (a) Si and (b) Ni.⁴⁰ Solid lines represent the experimental REELS spectra. Dotted lines show the components due to electrons undergo single surface excitation event in the relevant REELS spectrum, which are deduced by the partial intensity approach. Dashed lines represent the theoretically calculated DSEP using Tung's model.¹² For a better comparison, the theoretical curves were normalized in their maximum to the experimental data. (Reprinted from Ref. 40, Copyright (2005), with permission from Elsevier.)

is in a close agreement with the theoretical result. In contrast, the agreement is not so good for Ni. This must be attributed to deficiencies in the optical data for Ni, which is used to calculate $L_{n_b}(\Delta E)$.⁴⁰

Figure 14 shows the total SEP values for Si, Ni, Ge and Ag determined from the REELS spectra (shown in Fig. 13 for Si

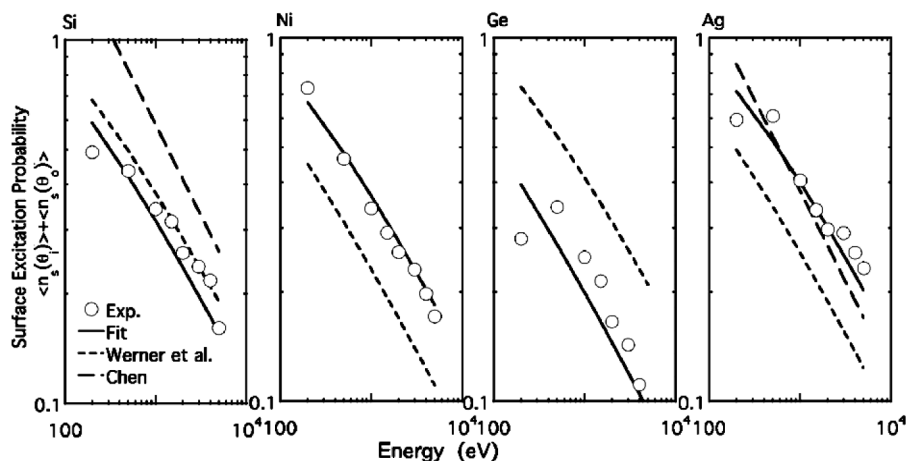


Fig. 14 SEP values for Si, Ni, Ge and Ag determined by the partial intensity approach.⁴⁰ The vertical axis shows the total SEP given as a sum of the SEPs for incoming and outgoing electrons in the REELS measurement. Open circles show SEPs determined from the REELS spectra (see Fig. 13 for Si and Ni) by the partial intensity approach. Solid curves are obtained by fitting Eq. (20) to open circles. a/a_{NFE} for Si, Ni, Ge, and Ag in Eq. (20) are 1.2, 1.0, 2.1, and 0.9,⁴⁰ where a_{NFE} is $0.171 \text{ eV}^{-1/2}$. Short dashed curves show SEPs calculated using Eq. (20) with a/a_{NFE} for Si, Ni, Ge, and Ag of 1.0, 1.8, 0.9, and 1.6 reported in Ref. 17. Long dashed curves show the SEP values calculated using Eq. (21) with a^* for Si and Ag of 2.5 and 2.53 reported in Ref. 11. (Reprinted from Ref. 40, Copyright (2005), with permission from Elsevier.)

and Ni) by the partial intensity approach.⁴⁰ For a comparison, the SEP values calculated by the empirical equations,

$$P_s(E, \alpha) = \frac{1}{a\sqrt{E\cos\alpha + 1}}, \quad (20)$$

$$P_s(E, \alpha) = \frac{a^*}{\sqrt{E\cos\alpha}}, \quad (21)$$

are shown, where a and a^* are the material parameters. Equation (20) is the modified version of the Oswald's equation proposed by Werner *et al.* (Werner-type equation).^{17,20} Equation (21) is the so-called Chen's type equation.¹¹ It is found that the SEP, *i.e.*, the average number of surface excitation events experienced by REELS electrons during a single surface crossing, exhibits a significant scatter when they are compared with those from different sources.

In the partial-intensity approach, when SEP and DSEP are retrieved from a REELS spectrum, the IMFP, λ_{in} , and the normalized DIMFP (DIMFP normalized to unit area, see Eq. (18)), $\lambda_{\text{in}}K_{\text{b}}(E, \Delta E)$, are required as input parameters describing inelastic scattering processes. Recently, the partial-intensity approach has been extended to determine the DIMFP and DSEP simultaneously from two REELS spectra, which are measured at the different primary energy of electrons, with the estimate for the IMFP,⁴³ and further extended to determine the optical constant.⁴⁴⁻⁴⁷

Figure 15 shows an example of the simultaneous determination of the DIMFP and DSEP for Cu from two REELS spectra measured at the primary energy of 1000 and 3000 eV by the partial intensity approach.⁴⁴ In the figure, the normalized DIMFP and DSEP retrieved from two REELS spectra are plotted by open and solid circles, respectively. Since the DIMFP and DSEP are expressed by Eqs. (S3) (Supporting Information) and (9), a unique solution of the dielectric constant, $\varepsilon(k, \omega) = \varepsilon_1(k, \omega) + i\varepsilon_2(k, \omega)$, to fit the experimentally determined DSEP and DIMFP, can be determined. Figure 16 shows the dielectric

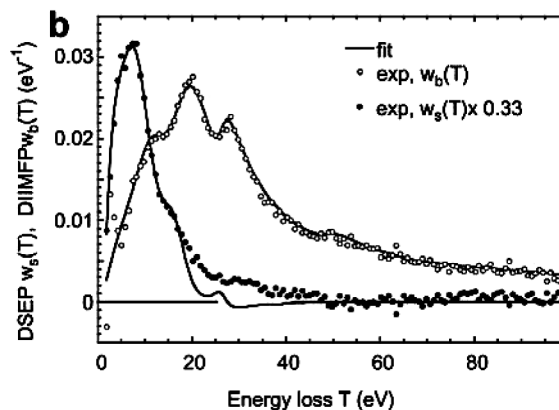


Fig. 15 Normalized DSEP (solid circles, $w_s(T)$ in this figure) and normalized DIMFP (open circles, $w_b(T)$ in this figure) experimentally determined from two REELS spectra measured at the primary energies of 1000 and 3000 eV for Cu by the partial intensity approach.⁴⁴ The solid line represents the calculated DSEP and DIMFP using the dielectric function shown in Fig. 16. (Reprinted from Ref. 44, Copyright (2006), with permission from Elsevier.)

function for Cu obtained by the partial-intensity approach.⁴⁴ The form of the dielectric function was the extended Drude-Lorentz model dielectric function⁴⁸ with a quadratic dispersion, which is given by Eq. (10). It is found that the resulting dielectric function shows reasonable overall agreements with Palik's data and those calculated by the density functional theory (DFT).⁴⁹ The partial-intensity approach is also believed to be an effective technique to determine the optical constant by the REELS measurement.

4-3 Absolute REELS analysis

Nagatomi *et al.* have also been involved in experimental and

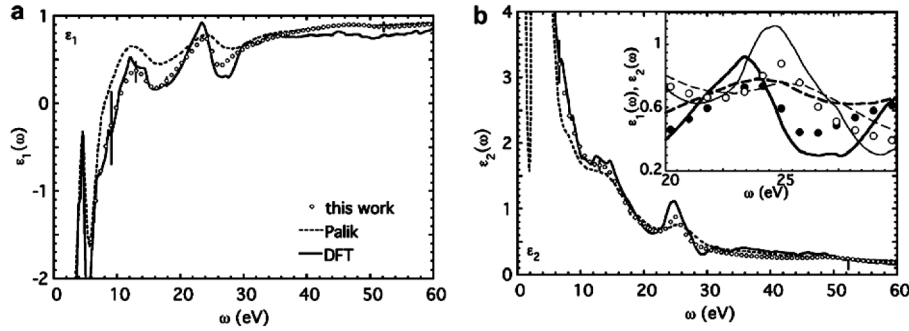


Fig. 16 (a) Real, $\epsilon_1(\omega)$, and (b) imaginary, $\epsilon_2(\omega)$, parts of the dielectric function for Cu retrieved from the REELS spectra by the partial-intensity approach.⁴⁴ Open and solid circles represent experimental $\epsilon_1(\omega)$ and $\epsilon_2(\omega)$, respectively. Thick and thin solid curves show $\epsilon_1(\omega)$ and $\epsilon_2(\omega)$ obtained by the density functional theory (DFT) calculation.⁴⁹ Thick and thin dashed lines represent the dielectric function calculated from the optical data by Palik.³⁷ (Reprinted from Ref. 44, Copyright (2006), with permission from Elsevier.)

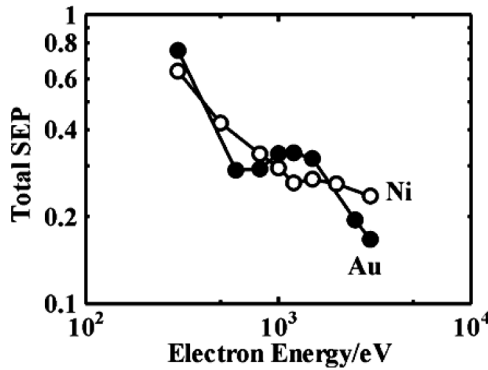


Fig. 17 Values of the total SEP for Ni (open circles) and Au (solid circles) giving as a sum of the SEPs for incoming and outgoing electrons in the REELS experiment determined by the absolute REELS analysis (see Ref. 58).

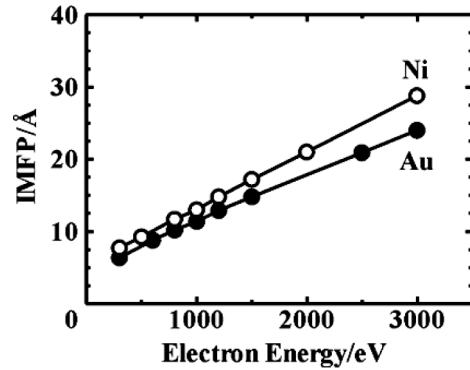


Fig. 18 IMFP values for Ni (open circles) and Au (solid circles) determined by the absolute REELS analysis (see Ref. 58).

theoretical investigations of the inelastic interaction of electrons with the solid surface,⁵⁰⁻⁵⁵ and have proposed an analytical approach to determine the IMFP, SEP and DSEP simultaneously from one absolute REELS spectrum.^{13,56} The application of this approach to several elements and the MC simulation study of the electron energy loss processes using the derived IMFP, SEP, and DSEP were also investigated.^{13,56-59} In this article, we briefly introduce their approach and obtained results.

In the absolute REELS analysis, a REELS spectrum is deconvoluted into components due to electrons participating in m -fold bulk and l -fold surface excitation events according to an equation,^{13,56}

$$J(s) = F(s) \sum_{m=0}^{\infty} \alpha_m [\lambda_{in} K_b(s)]^m \sum_{l=0}^{\infty} P_s^{\text{total},l} [K_s^{\text{in}}(s) P_s^{\text{in}}]^l, \quad (22)$$

where $J(s)$ and $F(s)$ are the Fourier transform of a measured REELS spectrum $J(E)$ and the energy distribution of primary electrons $F(E)$, respectively. The Σ term with respect to the summation over m denotes the electron transport in the bulk, *i.e.*, the angular deflection by elastic scattering and the energy loss processes due to bulk excitations. m is the number of bulk excitation events. α_m describes the probability that primary electrons undergo m -fold bulk excitation events in the solid

before being emitted from the surface. $K_b(s)$ is the Fourier transform of the DIMFP for bulk excitation, $K_b(E, \Delta E)$. The Σ term with respect to the summation over l describes the energy-loss processes due to surface excitations. $P_s^{\text{total},l}$ is the probability that electrons participate in l -fold surface excitation events. $K_s^{\text{in}}(s)$ is the Fourier transform of the DSEP for incoming electrons, $K_s^{\text{in}}(E, \Delta E)$, and P_s^{in} is the SEP for incoming electrons. In the absolute REELS analysis, absolutely measured REELS spectra by the noble CMA^{7,8} were analyzed. Input data describing the inelastic collision of electrons, which is required for the absolute REELS analysis, is only the normalized DIMFP describing the energy loss distribution by single bulk excitation event, $\lambda_{in} K_b(E, \Delta E)$. Since the intensity of REELS spectra is given with absolute units, a unique set of IMFP, SEP, and DSEP satisfying Eq. (22) can be obtained by the iteration procedure. Note that the multiple scattering events are taken into account in the absolute REELS analysis, as that for the partial intensity analysis, by calculating α_m using the MC simulation.

Figures 17 and 18 show the SEP and IMFP values for Ni and Au, respectively, determined by the absolute REELS analysis (see Ref. 58). From Fig. 17, it is found that the SEPs for Au and Ni are similar each other. The SEPs for Ni and Au are found to be close to those calculated by the predictive equation proposed by Werner *et al.* (for Ni, Ref. 40; for Au, Ref. 17). With respect to the IMFP values, the IMFP for Au is shorter

than that of Ni as expected. A comparison of the IMFP determined by the absolute REELS analysis with those calculated by the TPP-2M predictive equation revealed that the root-mean-square differences¹ between the absolutely determined IMFPs and those calculated by the TPP-2M equation were 3.1 Å for Ni and 2.2 Å for Au. The results confirmed that the absolutely determined IMFP values are in good agreement with those calculated by the TPP-2M equation. Further application of the absolute REELS analysis to other systems and investigations of the inelastic interaction of electrons with the solid surface are underway.

5 Summary

In this article, the basics of the study of surface excitations by the EPES analysis and the background shape analysis of the REELS spectrum are reviewed. From a viewpoint of the background shape analysis, the analysis of the background of the REELS spectrum is mainly focused on background subtraction of the spectrum and the extraction of information on the interaction between electrons and the solid surface. Since the most important issue is the peak intensity in the conventional quantitative analysis, the accuracy of background subtraction seems to be most essential. However, the effects of surface excitation is significant, and, for instance, because of the dependence of the contribution of surface excitations on the electron energy; therefore, it is considered that surface excitations play an important role in quantitative analysis. This means that the contribution of surface excitations should be taken into account in quantitative analysis.

At present, accurate quantitative and analytical treatments of surface excitations in surface electron spectroscopies are rather difficult because of multiple scattering undergone by signal electrons. In addition, surface excitations strongly depend on elements consisting of a sample. Furthermore, in the case of alloys and compounds, surface excitations are strongly affected by the composition and chemical state. Moreover, even though the elemental solid is treated, surface excitations may be affected by contamination on the surface. Therefore, understanding surface excitation phenomena is essential in order to improve the accuracy of the quantitative analysis. For this purpose, the development of the analytical method and simulator, and the construction of a database of scattering parameters have high potential. For further improvement in the accuracy of the quantitative analysis, not only an academic understanding of the surface excitation, but also an extension of understanding of practical applications are essential.

6 Acknowledgements

This work is partially supported by Grant-in-Aid from the Ministry of Education, Culture, Sports, Science and Technology, Japan (No. 21686005).

7 Supporting Information

The basic concept to understand the EPES analysis and the REELS analysis are described in Supporting Information. Information comes in useful to calculate values of the IMFP and SEP using predictive equations is also provided in Supporting Information. This material is available free of charge on the Web at <http://www.jsac.or.jp/analsci/>.

8 References

1. C. J. Powell and A. Jablonski, *J. Phys. Chem. Ref. Data*, **1999**, 28, 19.
2. C. J. Powell and A. Jablonski, *Surf. Interface Anal.*, **2000**, 29, 108.
3. G. Gergely, *Prog. Surf. Sci.*, **2002**, 71, 31.
4. W. S. M. Werner, C. Tomastik, T. Cabela, G. Richter, and H. Störi, *Surf. Sci.*, **2000**, 470, L123.
5. W. S. M. Werner, C. Tomastik, T. Cabela, G. Richter, and H. Störi, *J. Electron Spectrosc. Relat. Phenom.*, **2001**, 113, 127.
6. S. Tanuma, S. Ichimura, and K. Goto, *Surf. Interface Anal.*, **2000**, 30, 212.
7. K. Goto, N. Sakakibara, Y. Takeichi, Y. Numata, and Y. Sakai, *Surf. Interface Anal.*, **1994**, 22, 75.
8. K. Goto, N. Sakakibara, and Y. Sakai, *Microbeam Anal.*, **1993**, 2, 123.
9. Y. F. Chen, *Surf. Sci.*, **1996**, 345, 213.
10. Y. F. Chen and C. M. Kwei, *Surf. Sci.*, **1996**, 364, 131.
11. Y. F. Chen, *Surf. Sci.*, **2002**, 519, 115.
12. C. J. Tung, Y. F. Chen, C. M. Kwei, and T. L. Chou, *Phys. Rev. B*, **1994**, 49, 16684.
13. T. Nagatomi and K. Goto, *Phys. Rev. B*, **2007**, 75, 235424.
14. S. Tanuma, T. Shiratori, T. Kimura, K. Goto, S. Ichimura, and C. J. Powell, *Surf. Interface Anal.*, **2005**, 37, 833.
15. J. Zemek, P. Jiricek, B. Lesiak, and A. Jablonski, *Surf. Sci.*, **2003**, 531, L335.
16. G. Gergely, M. Menyhard, S. Gurban, J. Toth, and D. Varga, *Surf. Interface Anal.*, **2004**, 36, 1098.
17. W. S. M. Werner, W. Smekal, C. Tomastik, and H. Störi, *Surf. Sci.*, **2001**, 486, L461.
18. S. Tanuma, C. J. Powell, and D. R. Penn, *Surf. Interface Anal.*, **1991**, 17, 911.
19. Y. F. Chen, *Surf. Sci.*, **1997**, 380, 199.
20. R. Oswald, Ph. D. Thesis, Eberard-Karls-Universität, **1992**, Tübingen.
21. S. Gurban, G. Gergely, J. Toth, D. Varga, A. Jablonski, and M. Menyhard, *Surf. Interface Anal.*, **2006**, 38, 624.
22. S. Tougaard and I. Chorkendorff, *Phys. Rev. B*, **1987**, 35, 6570.
23. S. Tougaard and J. Kraaer, *Phys. Rev. B*, **1991**, 43, 1651.
24. G. Gergely, M. Menyhard, S. Gurban, A. Sulyok, J. Toth, D. Varga, and S. Tougaard, *Solid State Ionics*, **2001**, 141 - 142, 47.
25. G. Gergely, M. Menyhard, S. Gurban, A. Sulyok, J. Toth, D. Varga, and S. Tougaard, *Surf. Interface Anal.*, **2002**, 33.
26. S. Gurban, G. Gergely, M. Menyhard, J. Adam, M. Adamik, Sc. Daroczi, J. Toth, D. Varga, A. Csik, and B. Gruzza, *Surf. Interface Anal.*, **2002**, 34, 206.
27. S. Tougaard, *Solid State Commun.*, **1987**, 61, 547.
28. H. Jin, H. Yoshikawa, H. Iwai, S. Tanuma, and S. Tougaard, *J. Surf. Anal.*, **2009**, 15, 321.
29. H. Jin, H. Yoshikawa, H. Iwai, S. Tanuma, and S. Tougaard, *e-J. Surf. Sci. Nanotech.*, **2009**, 7, 199.
30. J. Jin, H. Yoshikawa, H. Iwai, S. Shinotsuka, S. Tanuma, and S. Tougaard, in Abstract of 13th European Conference on Application of Surface and Interface Analysis (ECASIA'09), Antalya, Turkey, October 18 - 23, **2009**, 238.
31. F. Yubero, J. M. Sanz, B. Ramskov, and S. Tougaard, *Phys. Rev. B*, **1996**, 53, 9719.
32. F. Yubero, D. Fujita, B. Ramskov, and S. Tougaard, *Phys. Rev. B*, **1996**, 53, 9728.
33. S. Hajati, O. Romanyuk, J. Zemek, and S. Tougaard, *Phys.*

- Rev. B*, **2008**, 77, 155403.
34. S. Hajati, O. Romanyuk, J. Zemek, and S. Tougaard, *Phys. Rev. B*, **2008**, 77, 24904(E).
35. T. J. Moravec, J. C. Rife, and D. L. Dexter, *Phys. Rev. B*, **1976**, 13, 3297.
36. V. P. Shirokovskii, M. M. Kirillova, and N. A. Shilkova, *Sov. Phys. JETP*, **1982**, 55, 464; *Zh. Eksp. Teor. Fiz.*, **1982**, 82, 784.
37. D. W. Lynch and W. R. Hunter, in “*Handbook of Optical Constants of Solids*”, ed. E. D. Palik, **1985**, Chap. 2.1.III, Academic, New York.
38. W. S. M. Werner, *Surf. Sci.*, **2003**, 526, L159.
39. W. S. M. Werner, *Surf. Interface Anal.*, **2003**, 35, 347.
40. W. S. M. Werner, L. Köver, S. Egri, J. Tóth, and D. Varga, *Surf. Sci.*, **2005**, 585, 85.
41. W. S. M. Werner and P. Schattschneider, *J. Electron Spectrosc. Relat. Phenom.*, **2005**, 143, 65.
42. W. S. M. Werner, in “*Surface Analysis by Auger and X-Ray Photoelectron Spectroscopy*”, ed. D. Briggs and J. T. Grant, **2003**, Chap. 10, IM Publications, Chichester, UK.
43. W. S. M. Werner, *Phys. Rev. B*, **2006**, 74, 075421.
44. W. S. M. Werner, *Surf. Sci.*, **2006**, 600, L250.
45. W. S. M. Werner, *Appl. Phys. Lett.*, **2006**, 89, 213106.
46. W. S. M. Werner, *Surf. Sci.*, **2007**, 601, 2125.
47. W. S. M. Werner, M. R. Went, M. Vos, K. Glantschnig, and C. Ambrosch-Draxl, *Phys. Rev. B*, **2008**, 77, 161404(R).
48. Y. F. Chen, C. M. Kwei, and C. J. Tung, *Phys. Rev. B*, **1993**, 48, 4373.
49. C. Ambrosch-Draxl and J. O. Sofo, *Comput. Phys. Commun.*, **2006**, 175, 1.
50. T. Nagatomi, Z.-J. Ding, and R. Shimizu, *Surf. Sci.*, **1996**, 359, 163.
51. T. Nagatomi, T. Kawano, and R. Shimizu, *J. Appl. Phys.*, **1998**, 83, 8016.
52. T. Nagatomi, T. Kawano, H. Fujii, E. Kusumoto, and R. Shimizu, *Surf. Sci.*, **1998**, 416, 184.
53. T. Nagatomi, R. Shimizu, and R. H. Ritchie, *J. Appl. Phys.*, **1999**, 85, 4231.
54. T. Nagatomi, R. Shimizu, and R. H. Ritchie, *Surf. Sci.*, **1999**, 419, 158.
55. T. Nagatomi, Y. Takai, B. V. Crist, K. Goto, and R. Shimizu, *Surf. Interface Anal.*, **2003**, 35, 74.
56. T. Nagatomi and K. Goto, *Appl. Phys. Lett.*, **2005**, 87, 224107.
57. T. Nagatomi and K. Goto, *Surf. Interface Anal.*, **2008**, 40, 1755.
58. T. Nagatomi and K. Goto, *Appl. Surf. Sci.*, **2009**, 256, 1200.
59. T. Nagatomi and K. Goto, *J. Electron Spectrosc. Relat. Phenom.*, **2009**, doi: 10.1016/j.elspec.2009.05.006.
-